RESEARCH ARTICLE



Transfer of stress from the 2004 Mw9.2 Sumatra subduction earthquake promoted widespread seismicity and large strikeslip events in the Wharton Basin

Laiyin Guo^{1,5} | Jian Lin^{2,3,4,5} | Fan Zhang^{2,3} | Zhiyuan Zhou^{2,3}

²Key Laboratory of Ocean and Marginal Sea Geology, South China Sea Institute of Oceanology, Innovation Academy of South China Sea Ecology and Environmental Engineering, Chinese Academy of Sciences, Guangzhou, China

³Southern Marine Science and Engineering Guangdong Laboratory (Guangzhou), Guangzhou, China

⁴Department of Geology and Geophysics, Woods Hole Oceanographic Institution, Woods Hole, MA, USA

⁵Department of Ocean Science and Engineering, Southern University of Science and Technology, Shenzhen, China

Correspondence

Jian Lin, Department of Geology and Geophysics, Woods Hole Oceanographic Institution, Woods Hole, MA 02543, USA. Email: jlin@whoi.edu

Fan Zhang, Key Laboratory of Ocean and Marginal Sea Geology, South China Sea Institute of Oceanology, Chinese Academy of Sciences, Guangzhou 510301, China. Email: zhangfan@scsio.ac.cn

Funding information

Southern Marine Science and Engineering Guangdong Laboratory, Grant/Award Number: GML2019ZD0205; National Natural Science Foundation of China, Grant/ Award Number: 41890813, 91628301, 41976064 and 41976066; China-Pakistan Joint Research Center on Earth Sciences; Chinese Academy of Sciences, Grant/ Award Number: Y4SL021001, QYZDY-SSW-DQC005 and 133244KYSB20180029

Abstract

The 2004 Mw9.2 Sumatra and 2012 Mw8.6 Wharton Basin (WB) earthquakes provide the unprecedented opportunity to investigate stress transfer from a megathrust earthquake to the subducting plate. Comprehensive analyses of this study revealed that the 2004 earthquake excited widespread seismicity in the WB, especially in regions of calculated stress increase greater than 0.3 bars. The 2004 earthquake stressed all three rupture planes of the 2012 Mw8.6 strike-slip mainshock and the largest Mw8.2 aftershock with mean values of Coulomb stress between 0.3 and 2.1 bars. For the 77 Mw \geq 4 regional events since 2012, at least one nodal plane for 95% of the events, and both nodal planes for 72% of the events experienced stress increase due to the 2004 earthquake. Results of the analyses also revealed that the regional stress directions in the WB may have controlled the sub-fault orientations of the 2012 Mw8.6 strike-slip earthquake.

¹School of Ocean and Earth Science, Tongji University, Shanghai, China

1 | INTRODUCTION

The 26 December 2004 Mw9.2 earthquake ruptured 1,200-1,600 km of the Sumatra subduction zone (Ammon et al., 2005; Lay et al., 2005). An increase in seismicity was reported in the Wharton Basin (WB) following the 2004 earthquake (Delescluse et al., 2012). Eight years later, the 11 April 2012 Mw8.6 earthquake struck the WB and was ~310 km seaward of the epicentre of the 2004 earthquake (Lay, 2019). This largest instrument-recorded strike-slip event was followed approximately 2 hr later with the Mw8.2 strike-slip aftershock (Figure 1). These events provide the unprecedented opportunity to investigate stress transfer and the triggering of seismicity in the subducting plate following a great subduction zone earthquake.

The 2012 Mw8.6 mainshock consisted of multiple sub-faults, as revealed by investigations using back-projection analysis (Ishii, Kiser, & Geist, 2013; Meng et al., 2012; Wang, Mori, & Uchide, 2012), W-phase inversion (Duputel et al., 2012), and finite fault modelling (Hill et al., 2015; Wei, Helmberger, & Avouac, 2013; Yue, Lay, & Koper, 2012). These analyses reveal that the conjugate strike-slip faults are oriented NNE and NWW, respectively. The finite fault model (FFM) from Wei et al. (2013) consists of three sub-faults with fault lengths of \sim 260 (F1), 420 (F2), and 420 km (F3) (Figure 2).

The WB is on the eastern end of the Indian Plate and subducting under the Eurasian Plate at an average convergence rate of 4.7–5.7 cm/year (Carton et al., 2014). The crustal age in the WB

is 40–80 Ma (Liu, Curray, & McDonald, 1983; Singh et al., 2017). Seafloor spreading created a distinctive set of high-angle, left-lateral-offset fossil fracture zones with strikes of ~6° (Figure 2; Jacob, Dyment, & Yatheesh, 2014). It has been suggested that the seismicity in the WB could be the result of fracture zone reactivation (Deplus et al., 1998; Robinson, Henry, Das, & Woodhouse, 2001). However, both the location and strike of the 2012 sub-faults differ significantly from the fossil fracture zones (Figure 2). This suggests that the 2012 Mw8.6 earthquake instead occurred on previously unidentified conjugate faults.

Several studies indicate that the 2004 subduction earthquake has caused significant stress changes in the WB (Fan & Shearer, 2016; Sevilgen, Stein, & Pollitz, 2012; Zhang, Chen, & Ge, 2012). For example, it has been suggested that a reduction in normal stress due to the 2004 earthquake resulted in the 2012 Mw8.6 earthquake (Ishii et al., 2013). However, the magnitude and spatial variation of the large-scale stress change in the WB and specific effects on individual faults are still poorly quantified.

This study comprehensively investigated the stress transfer to the WB from the 2004 Sumatra subduction earthquake. Our investigation focused on the stressing in different zones and for different types of ruptures in the WB: (a) The three sub-faults of the 2012 Mw8.6 mainshock; (b) the rupture plane of the largest 2012 Mw8.2 aftershock; and (c) the 77 Mw \geq 4 regional events after the 2012 events with focal mechanism solutions.

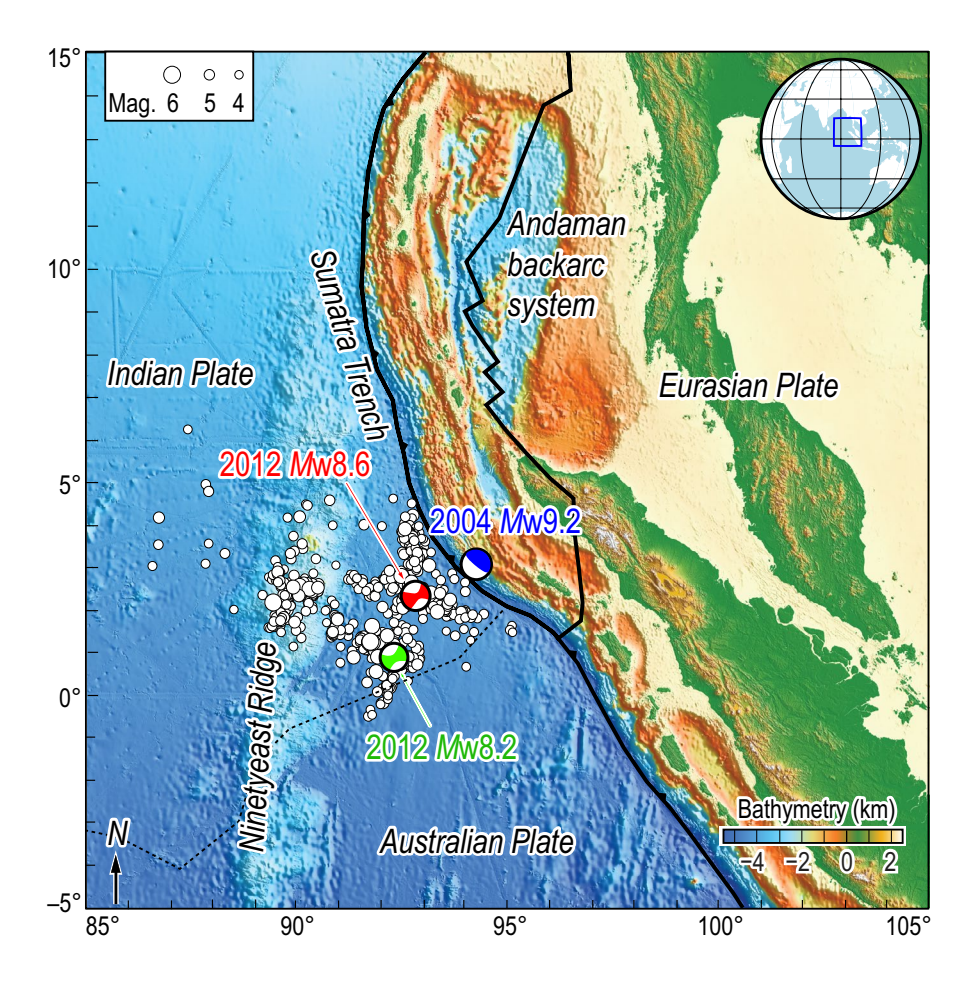


FIGURE 1 Map view of the 2004 Mw9.2 Sumatra subduction earthquake (blue focal mechanism), the 2012 Mw8.6 strike-slip earthquake (red focal mechanism), and the largest 2012 Mw8.2 aftershock (green focal mechanism) in the Wharton Basin. The subduction zone plate boundary (solid black lines) and the hypothesized Indo-Australian plate boundary (dashed black lines) are from Bird (2003). Seismicity (solid white dots) during 04/11/2012-11/01/2019 is from the USGS catalogue (https://earthquake. usgs.gov/earthquakes/search) [Colour figure can be viewed at wileyonlinelibrary. com]

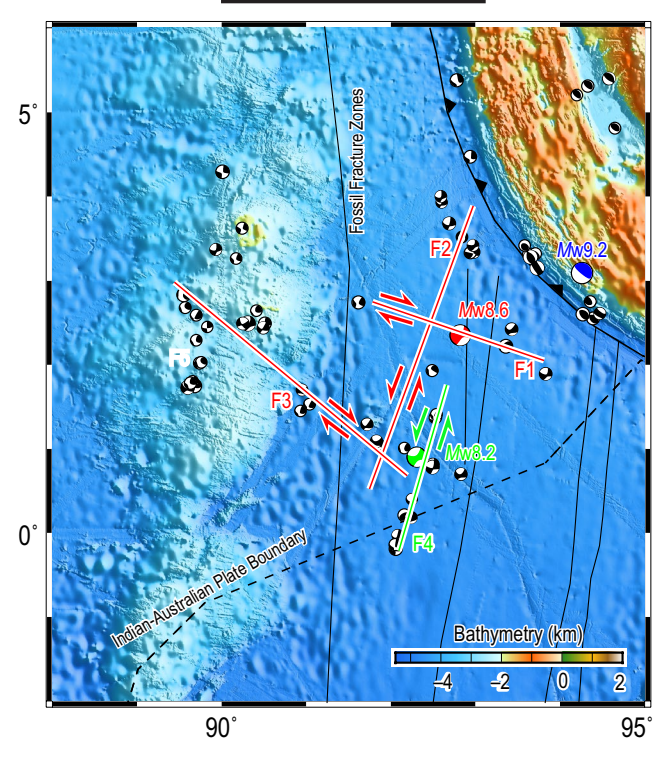


FIGURE 2 Focal mechanisms of 77 Mw \geq 4 regional events since 2012. The focal mechanism solutions are from global centroid moment tensor catalogue (https://www.globalcmt.org/CMTfiles. html; Dziewoński, Chou, & Woodhouse, 1981; Ekström et al., 2012). Black lines indicate fossil fracture zones in the Wharton Basin from Jacob et al. (2014). Dashed line indicates assumed plate boundary between the Indian and Australia Plates. The red lines indicate the three sub-faults of the Mw8.6 event, F1 (260 km), F2 (420 km) and F4 (420 km). The green line indicates the fault of the Mw8.2 event F4 (260 km), which was 2 hr later after the Mw8.6 event [Colour figure can be viewed at wileyonlinelibrary.com]

2 | CALCULATION OF COULOMB STRESS CHANGES

Changes in the Coulomb failure stress $\Delta \sigma_{\rm c}$ caused by a "source fault" earthquake is defined as follows:

$$\Delta \sigma_{\rm c} = \Delta \sigma_{\rm s} + \mu' \Delta \sigma_{\rm n},\tag{1}$$

where $\Delta\sigma_{\rm s}$ is the shear stress change on a given "receiver fault" plane (positive in the direction of receiver fault rake), $\Delta\sigma_{\rm n}$ is the normal stress change (positive for fault unclamping), and μ' is the effective friction coefficient, which includes the effects of pore pressure change (King & Cocco, 2001; Lin & Stein, 2004; Lin et al., 2011). In this study, changes in the Coulomb stress were calculated using the Coulomb 3.3 modelling software (Toda, Stein, Sevilgen, & Lin, 2011), which is suitable for modelling 3D stress and deformation in an elastic half-space.

Using the FFM for the 2004 Mw9.2 Sumatra earthquake (Chlieh et al., 2007; Sevilgen et al., 2012), we calculated $\Delta\sigma_{\rm c}$ for various types of interested receiver faults. Previous studies have shown that μ' ranges between 0 and 0.8, where $\mu'=0.4$ appears to be optimal for

modelling strike-slip faults (King, Stein, & Lin, 1994; Qiu & Chan, 2019; Toda, Stein, & Lin, 2011). The 2004 source fault consists of a set of sub-patches; here, we adopted a nine-patch solution that was obtained using the observed seismological and geodetic constraints (Sevilgen et al., 2012). We also used a higher-resolution FFM with many more sub-patches for the 2004 source fault; the results were similar to the nine-patch solution because much of the study region is located sufficiently far from the 2004 source earthquake (Figure 3). In modelling the Coulomb stress transfer related to the 2012 Mw8.6 earthquake, we considered three sub-faults F1, F2, and F3, with 156, 260, and 260 sub-patches, respectively (Table 1). The 2012 Mw8.2 aftershock was modelled using 299 sub-patches (Table 1).

3 | RESULTS

3.1 Overall pattern of stress change in the WB

We first examined the overall pattern of stress change in the WB caused by the 2004 earthquake. Stress changes were calculated for three types of potential receiver faults in the WB. (a) Distributed strike-slip receiver faults that are optimally oriented for Coulomb

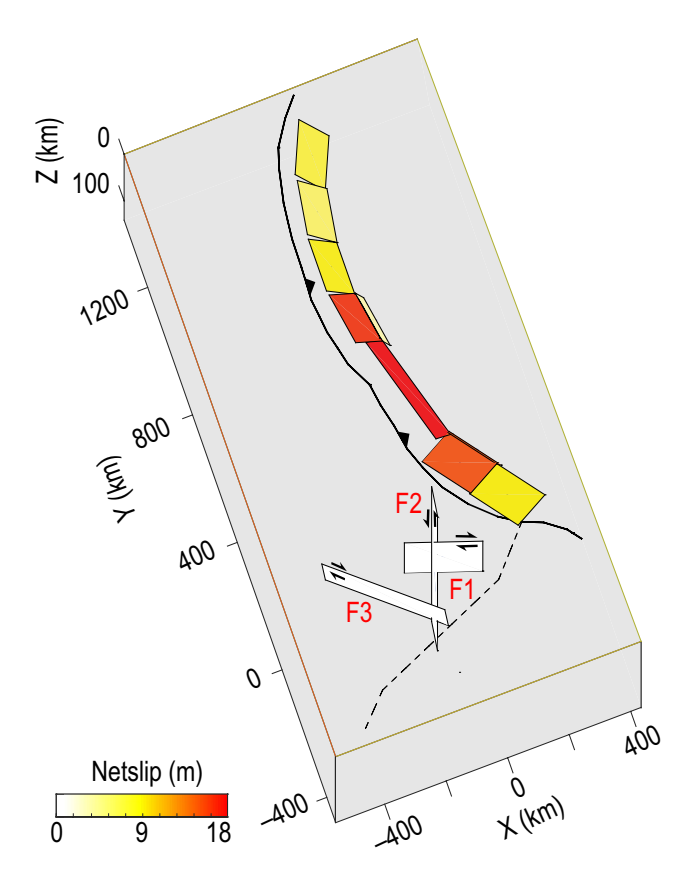


FIGURE 3 3D view of the 2004 Sumatra earthquake slip model from Sevilgen et al. (2012). Shown is a solution of nine sub-patches. The three sub-faults of the 2012 Mw8.6 earthquake, F1, F2, and F3, are also displayed [Colour figure can be viewed at wileyonlinelibrary.com]

TABLE 1 Parameters of earthquake faults used in the Coulomb stress transfer calculation

	Seismic moment	Number of patches	Netslip (m)			Parameters		
Earthquake			Min	Max	Average	Strike (°)	Dip (°)	Rake (°)
2004 Mw9.2	7.62e + 29	9	3.0	19.1	11.0	Variable	Variable	Variable
2012 Mw8.6	6.73e + 28							
F1		156	0.0	12.0	3.4	289	89	Variable
F2		260	0.0	28.0	4.8	20	74	Variable
F3		260	0.0	8.0	1.2	310	60	Variable
2012 Mw8.2	1.32e + 28	299	0.01	6.2	2.7	16	74	Variable

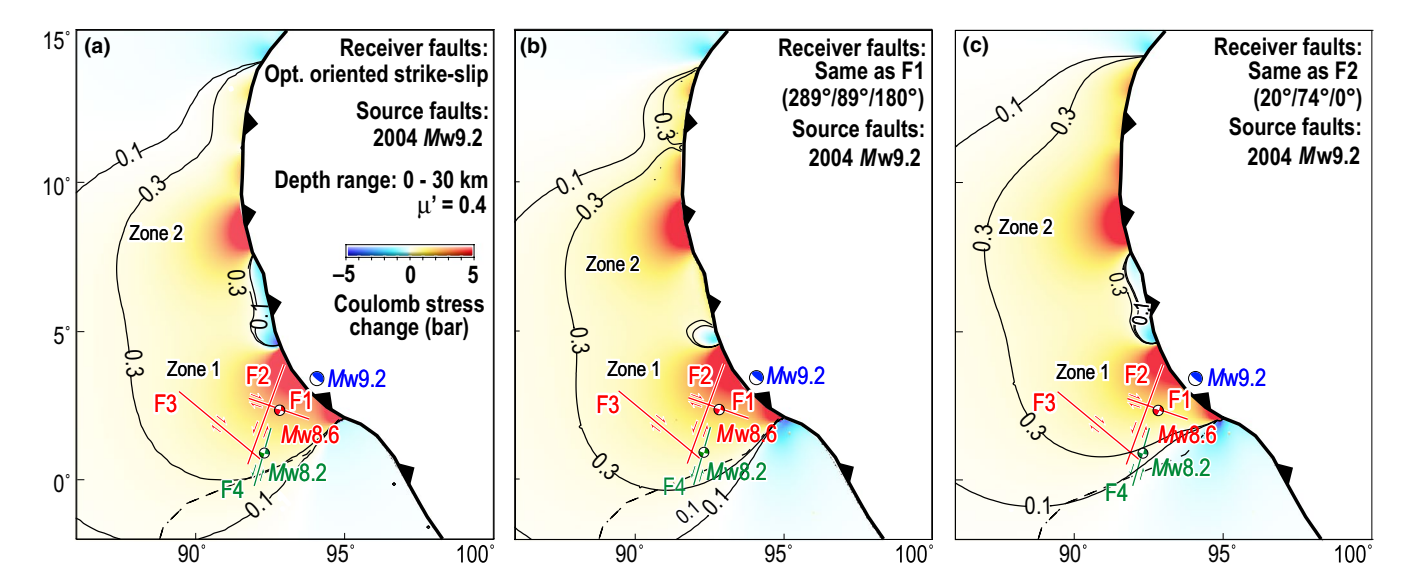


FIGURE 4 (a) Coulomb stress change caused by the 2004 subduction earthquake for optimally-oriented strike-slip receiver faults, assuming $\mu' = 0.4$. For a given map view point, the Coulomb stress changes for each 1 km depth interval for depth range of 0–30 km were calculated and the maximum value among the 30 depths is plotted. (b, c) Similar to panel (a), but assuming that the receiver faults have the same parameters of the 2012 sub-fault F1 (289°/89°/180°) (b) or sub-fault F2 (20°/74°/0°) (c) [Colour figure can be viewed at wileyonlinelibrary.com]

stress failure (Figure 4a). (b) Receiver faults with the same strike/dip/rake of F1 (289°/89°/180°; Figure 4b). (c) Receiver faults with the same strike/dip/rake of F2 (20°/74°/0°; Figure 4c).

The overall patterns of the stress changes in the WB are similar for the three types of receiver faults (Figure 4). The 2004 earthquake induced a strong stress increase in the southern (Zone 1) and northern (Zone 2) zones, which are separated by a region of relatively small stress change (Figure 4a). The three sub-faults of the 2012 mainshock (F1, F2, and F3) are all located in a region of Coulomb stress increase greater than 0.3 bars (Zone 1 in Figure 4). The seismicity was low during the 8 years (12/26/1996–12/25/2004) before the 2004 earthquake (Figure 5a). During the first 8 years (12/26/2004–04/10/2012) after the 2004 earthquake, the regional seismicity increased in both Zones 1 and 2, especially where the Coulomb stress increase was greater than 0.3 bars (Figure 5b; Figure S1). The increased regional seismicity in the WB was also reported by Delescluse et al. (2012), although thus far no events with magnitude greater than 6 had occurred in Zone 2. During the 8 years (04/11/2012–12/31/2019) after the 2012 earthquakes, the

seismicity in the WB was concentrated in the areas of Coulomb stress increase caused by both the 2004 and 2012 earthquakes (Figure 5c).

3.2 | Stress change on the sub-faults of the 2012 Mw8.6 mainshock

We further calculated the stressing from the 2004 earthquake on F1, F2, and F3 (Figure 6). The full length of F1 experienced increased shear (Figure 6a), normal (Figure 6b), and Coulomb (Figure 6c) stresses. The calculated $\Delta\sigma_c$ increase on F1 ranged from 1–2.5 bars (mean of 2.1 bars) (Figure 6c). The maximum $\Delta\sigma_c$ increase of 2.5 bars was located ~ 100 km from the northeast corner of F1 (Figure 6c). The full length of F2 also experienced increased shear (Figure 6e), normal (Figure 6f), and Coulomb (Figure 6g) stresses. The $\Delta\sigma_c$ on F2 increased rapidly from 0.2 to 6.9 bars approaching the northeast corner near the Sumatra Trench (Figure 6g) with a mean of 1.9 bars over F2.

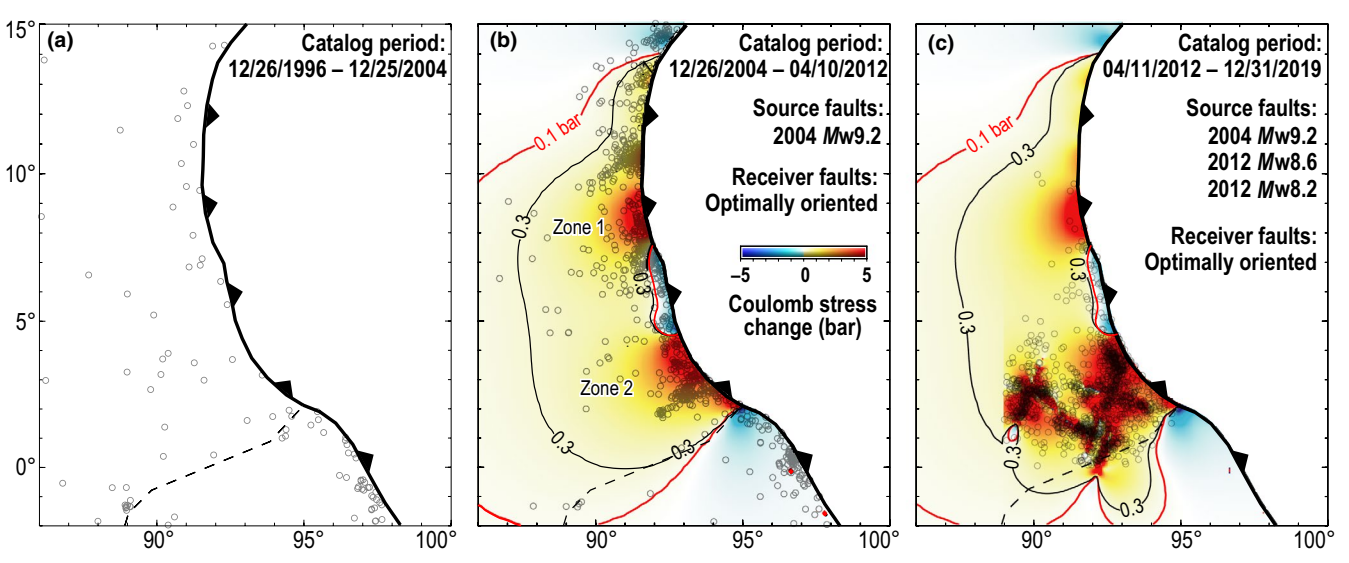


FIGURE 5 (a) Background seismicity (black circles) in the Wharton Basin (WB) during the 8 years (12/26/1996-12/25/2004) before the 2004 Mw9.2 thrust earthquake. (b) Calculated maximum Coulomb stress change on optimally oriented strike-slip receiver faults caused by the 2004 earthquake for the depth range of 0–30 km, assuming $\mu' = 0.4$. Also shown are aftershocks (black circles) in the WB during the 8 years (12/26/2004–04/10/2012) between the 2004 thrust earthquake and 2012 strike-slip mainshock. (c) Calculated maximum Coulomb stress change on optimally oriented strike-slip receiver faults caused by the combination of the 2004 earthquake and the 2012 events (Mw8.6 and Mw8.2) for depth range of 0–30 km. Also shown are aftershocks (black circles) during the 8 years (04/11/2012–12/31/2019) after the 2012 earthquakes [Colour figure can be viewed at wileyonlinelibrary.com]

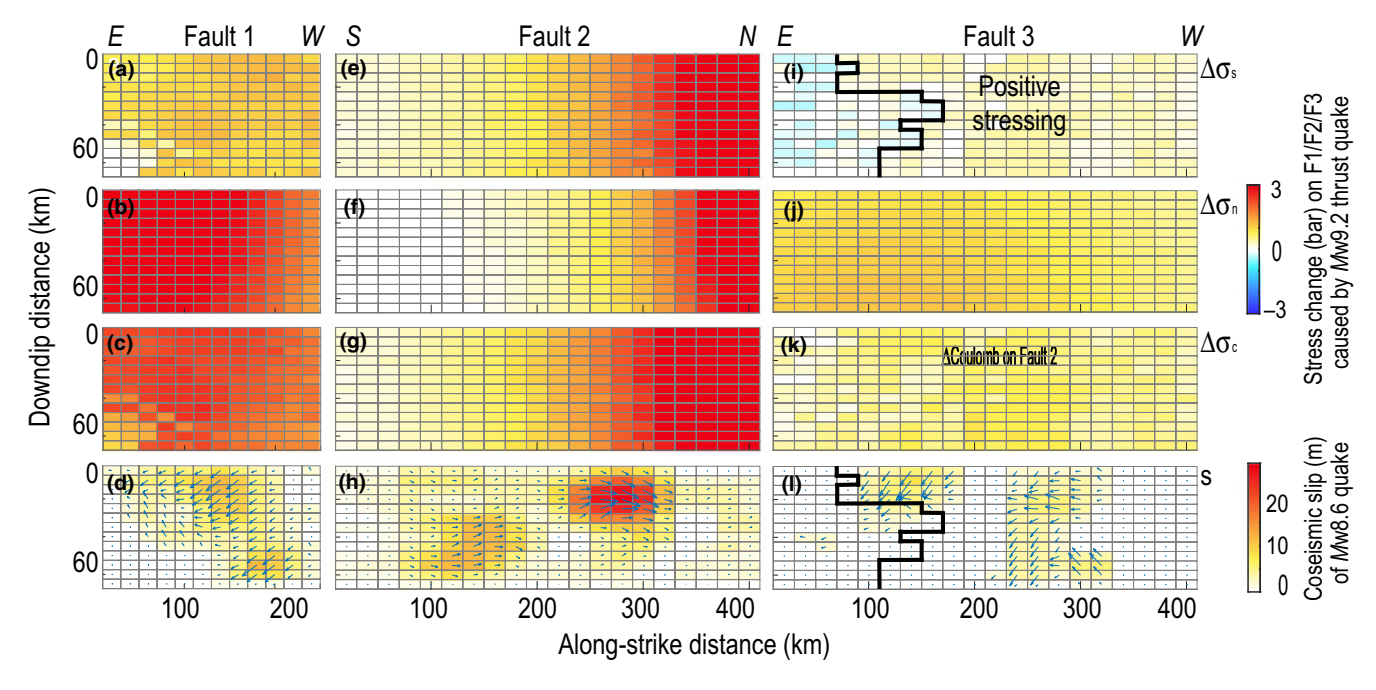


FIGURE 6 (a, e, i) Calculated shear stress changes caused by the 2004 earthquake on the 2012 sub-faults F1 (panel a), F2 (e), and F3 (i), respectively. (b, f, j) Calculated normal stress changes caused by the 2004 earthquake on the same sub-faults. (c, g, k) Calculated Coulomb stress changes caused by the 2004 earthquake. (d, h, l) Observed coseismic slip associated with the 2012 Mw8.6 earthquake on sub-faults F1 (d), F2 (h), and F3 (l; from Wei et al., 2013) [Colour figure can be viewed at wileyonlinelibrary.com]

The 2004 earthquake likewise had an increased normal stress on the full length of F3 (Figure 6j). However, only its western 2/3 experienced a moderate increase in shear stress, while its eastern 1/3 experienced a mild shear stress decrease

(Figure 6i). The entire F3 experienced an increase in normal stress (Figure 6j). The resultant Coulomb stress was positive over the full length of F3 and ranged from 0 to 0.9 bars (mean of 0.5 bars) (Figure 6k).

Thus, the three sub-faults of the 2012 mainshock are all located within regions of Coulomb stress increase (Figure 6c,g,k), which is consistent with the interpretation that the 2012 sub-fault planes were brought closer to failure due to the 2004 earthquake. Patches of the observed coseismic slip (Figure 6d, 6h, and 6l) correlate with areas of Coulomb stress increases (Figure 7). However, there is not a linear correlation between the magnitude of the stress changes and the amount of coseismic slip (Figure 7).

3.3 | Stress change on the rupture plane of the largest 2012 Mw8.2 aftershock

We calculated the stress changes on F4 caused by the 2004 earthquake and 2012 mainshock (Figure 8). The 2004 earthquake caused a

moderate increase in the shear stress (Figure 8a) and a relatively small change in the normal stress (Figure 8b), resulting in an overall increase in the Coulomb stress of 0-0.8 bars (mean of 0.3 bars) over the entire length of F4 (Figure 8c). This suggests that F4 was also brought closer to failure by the 2004 earthquake, similar to the cases of F1–F3.

Our calculations revealed that the 2012 mainshock caused a decreased shear stress over most of F4 (Figure 8e) and an increased normal stress over the southern 83% of the F4 length (Figure 8f). The resultant Coulomb stress change was negative over most of F4 (Figures 8g and 9). The previous study of Wu, Lei, Cai, and Li (2015) reported that the 2012 mainshock imparted the Coulomb stress on F4. The differences in the results between this study and Wu et al. (2015) may arise from the difference in the assumed FFM of the 2012 mainshock. The mainshock source model used in Wu et al. (2015) was an earlier model of a simplified single fault. The mainshock source model

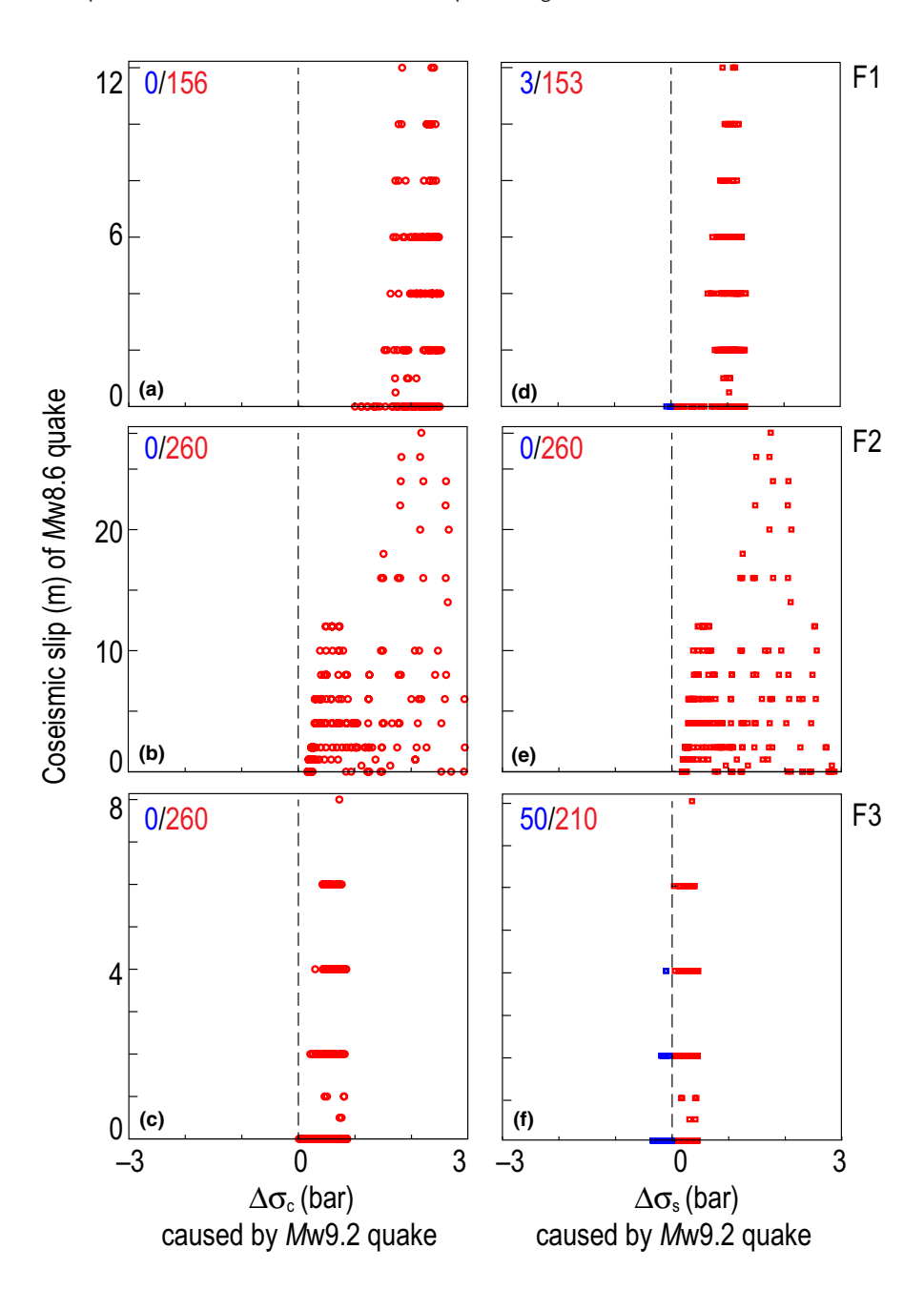


FIGURE 7 Calculated Coulomb stress change (a, b, c) and shear stress change (d, e, f) caused by the 2004 earthquake versus the observed coseismic slip (Wei et al., 2013) on every patch of the sub-faults F1, F2, and F3 of the 2012 Mw8.6 mainshock. The number in blue is the number of the patches that experienced negative stress changes while the number in red is the number of the patches that experienced increased stress changes [Colour figure can be viewed at wileyonlinelibrary.com]

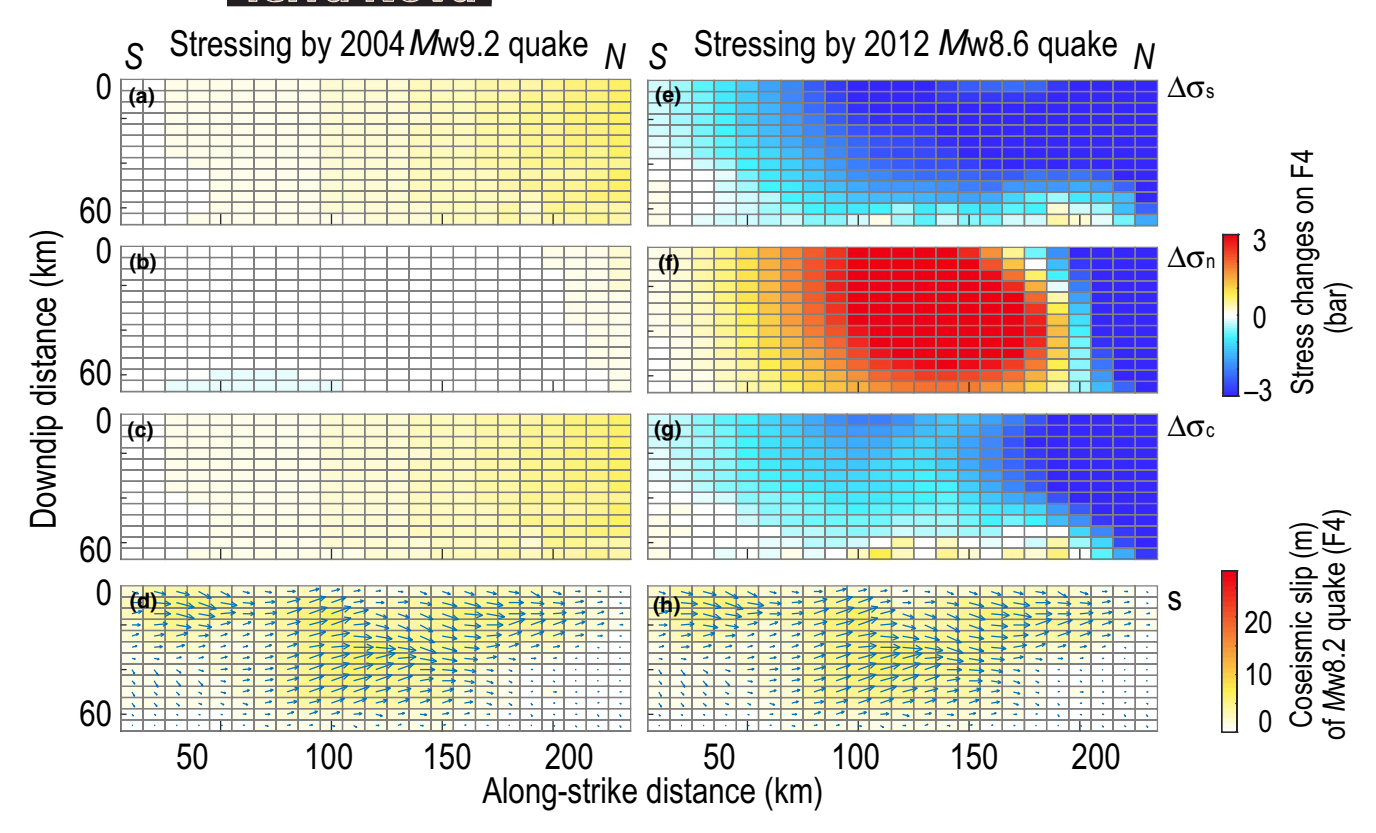


FIGURE 8 Calculated shear (a), normal (b), and Coulomb (c) stress changes caused by the 2004 Mw9.2 earthquake on the largest 2012 Mw8.2 aftershock fault plane F4, in comparison to the observed coseismic slip (d) on F4 (Wei et al., 2013). Calculated shear (e), normal (f), and Coulomb (g) stress changes caused by the 2012 Mw8.6 mainshock on the 2012 Mw8.2 aftershock fault plane F4 and the observed coseismic slip (h) on F4 [Colour figure can be viewed at wileyonlinelibrary.com]

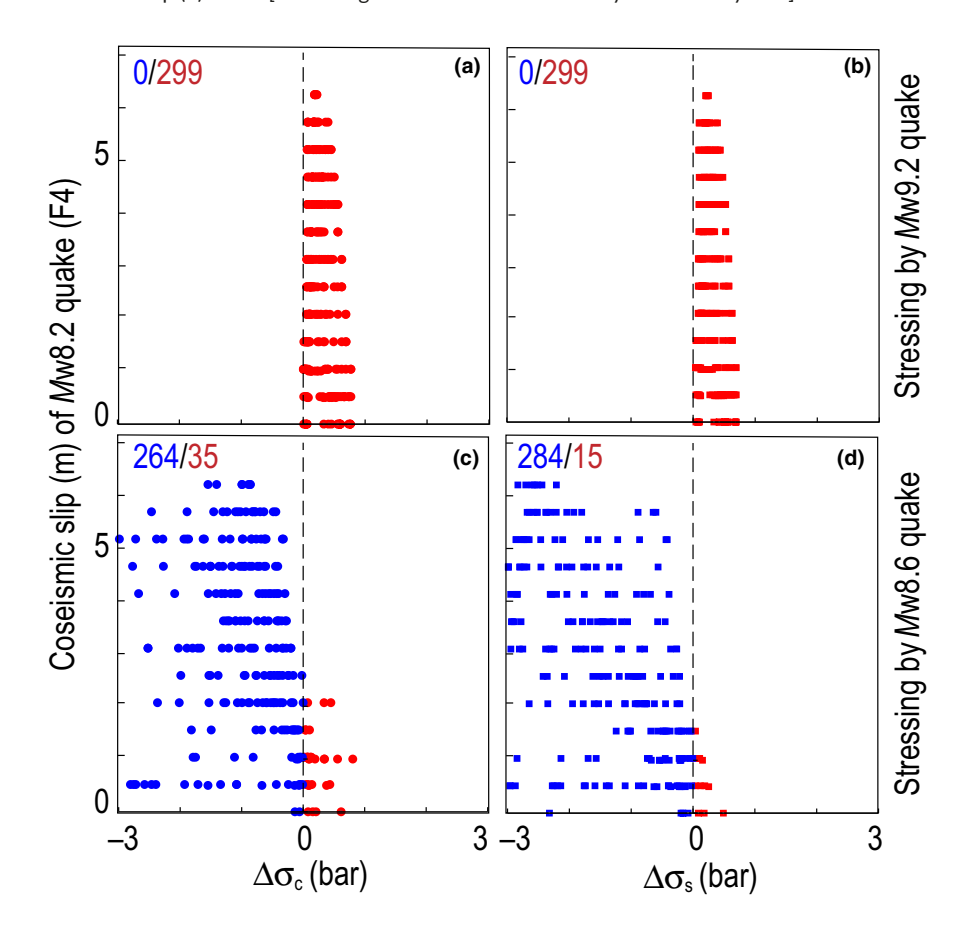
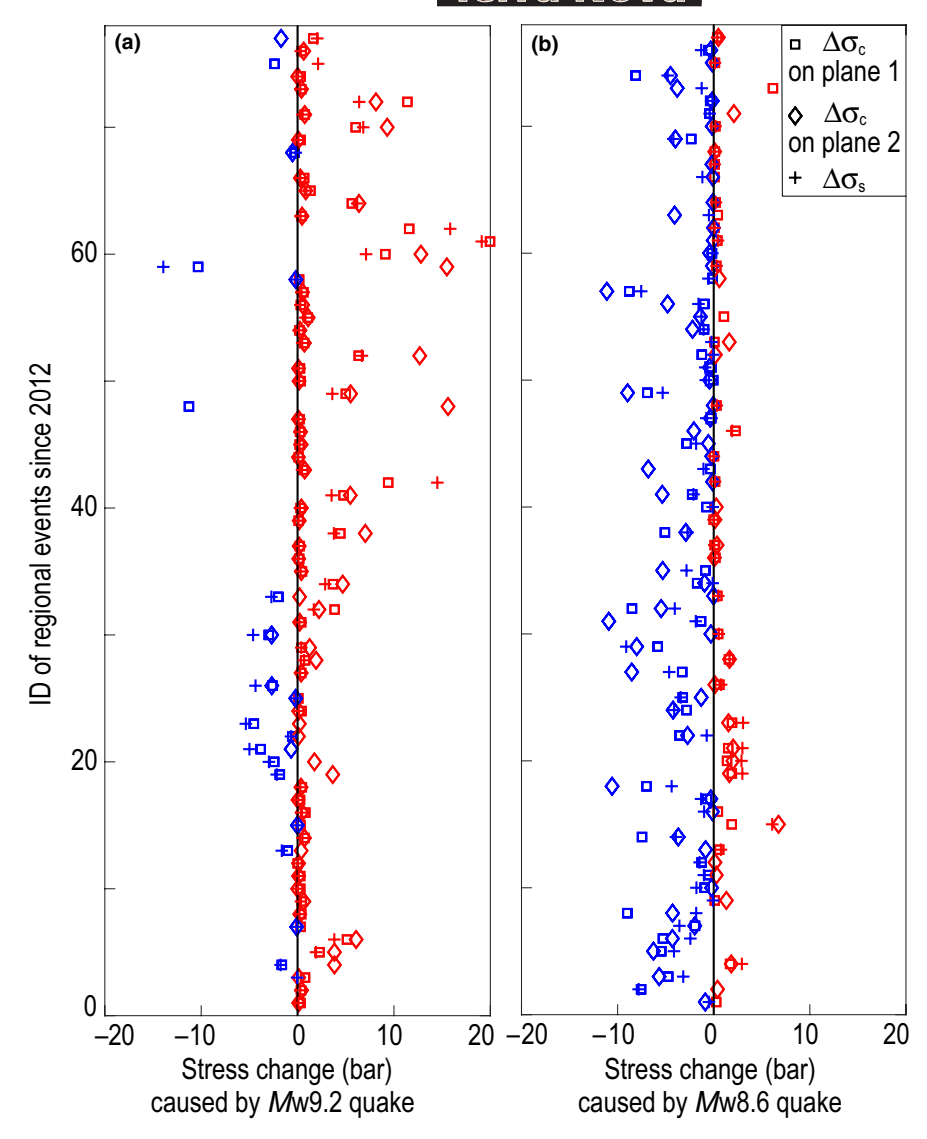


FIGURE 9 Calculated Coulomb (a) and shear (b) stress changes caused by the 2004 Mw9.2 earthquake on the 2012 Mw8.2 fault plane F4 versus the observed coseismic slip on F4 (Wei et al., 2013). Calculated Coulomb (c) and shear (d) stress changes caused by the 2012 Mw8.6 earthquake on the 2012 Mw8.2 fault plane F4 versus the observed coseismic slip on F4 [Colour figure can be viewed at wileyonlinelibrary.com]

FIGURE 10 Calculated stress changes caused by the 2004 Mw9.2 earthquake (a) and the 2012 Mw8.6 earthquake (b) on the nodal planes of the 77 Mw \geq 4 regional events with focal mechanisms after the 2012 main shock. Vertical axis marks the regional event number [Colour figure can be viewed at wileyonlinelibrary. com]



used in this study was more comprehensive, consisted of three conjugated sub-faults, and can better reproduce the seismic observations than the earlier single-fault source model.

Regardless the static stress relationship between the 2012 Mw8.6 mainshock and Mw8.2 aftershock, the dynamic stressing by the Mw8.6 mainshock may have contributed to the triggering of the Mw8.2 aftershock. Dynamic stress triggering of earthquakes has been extensively reported (Anderson, Aagaard, & Hudnut, 2003; Freed, 2005; Gomberg, Bodin, & Reasenberg, 2003; Hill et al., 1993). We noted that F4 was located at the southeastern end of F3 (Figure 2). Whether the directivity of F3 might favour the dynamic stress triggering of F4 remains a subject for future investigation.

3.4 | Stress changes on nodal planes of Mw ≥ 4 regional events with focal mechanisms

During the first 1.5 years (04/11/2012–11/22/2013) after the 2012 mainshock, 77 $Mw \ge 4$ events with focal mechanisms were observed in the study region (Ekström, Nettles, & Dziewoński, 2012; Figure 2).

We calculated the stress changes on the nodal planes of these regional events as caused by the 2004 Mw9.2 (Figure 10a) and 2012 Mw8.6 earthquakes (Figure 10b). The 2004 earthquake increased the Coulomb stress on at least one nodal plane for 95% of the events (73 out of 77), and both nodal planes for 72% of the events (55 out of 77) (Figure 10a). Thus, the 2004 earthquake may have promoted a range of regional events in the study region, including the 77 Mw \geq 4 events with focal mechanisms. The 2012 mainshock increased the Coulomb stress on at least one nodal plane of only 54% of the events (42 out of 77) (Figure 10b) and thus appeared to have much less influence on the regional events.

4 | DISCUSSION

4.1 | The role of regional stress in controlling the 2012 rupture plane orientation

According to the Coulomb stress transfer interpretation, the optimally-oriented fault directions at a given point should be controlled

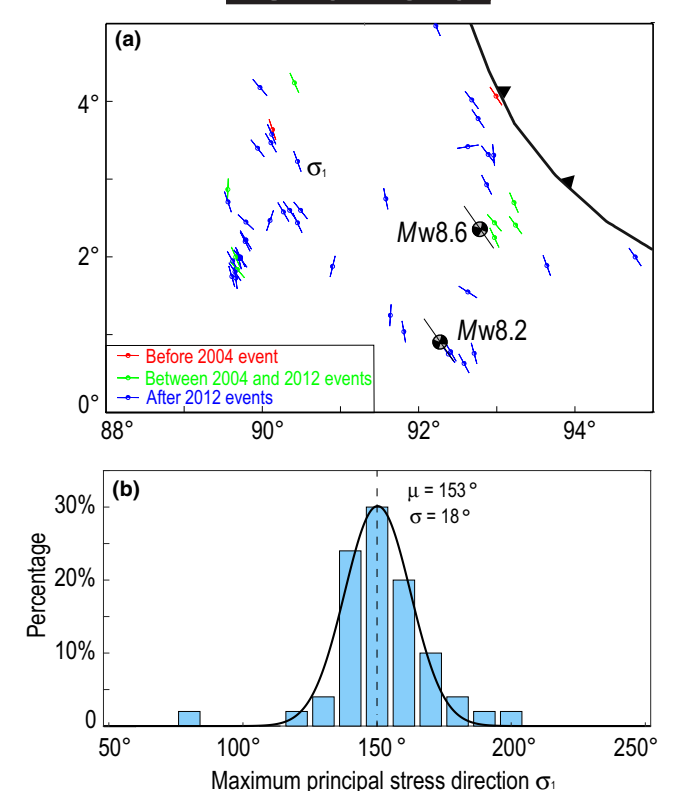


FIGURE 11 (a) Local maximum compressional principal stress directions calculated from focal mechanisms of 51 individual strike-slip earthquakes in the Wharton Basin during 1999–2015 (Heidbach et al., 2018). (b) Histogram of the observed local maximum compressional principal stress directions from the individual strike-slip earthquakes of panel (a), together with a Gaussian best-fitting curve (black line) [Colour figure can be viewed at wileyonlinelibrary.com]

by the combination of changes in the coseismic Coulomb stress $\Delta\sigma_c$ and regional stress field $\sigma_1/\sigma_2/\sigma_3$ (King et al., 1994). Heidbach et al. (2018) calculated the local stress orientations from 51 strikeslip regional events in the WB from 1999 to 2015 (Figure 11a). The directions of maximum compressional stress (σ_1) were in the range of 153°±18° (Figure 11b).

If the regional stress is negligible, the orientations of the optimum slip planes are controlled only by changes in the coseismic stress. We found that when the regional stress is negligible, the direction of maximum principle stress σ_1 on optimally oriented faults would vary greatly along F1 (83°–140°), F2 (10°–129°) and F3 (119°–148°; Figure 12a; Table 2). In contrast, for larger regional stresses, the direction of maximum principle stress σ_1 is much more consistent

along F1 (148.9°-150°), F2 (149.3°-150°), and F3 (150°; Figure 12b; Table 2).

Our calculations reveal that when the magnitude of the regional stresses reaches ~1.5 bars or greater, the predicted direction of maximum principle stress σ_1 becomes consistent along the length of the single sub-faults F1 (Figure 12c), F2 (Figure 12d), F3 (Figure 12e), and F4 (Figure 12f), which reflects the dominance of regional stresses at controlling fault directions in the study area. While the data are still relatively limited, studies have estimated the magnitude of regional stresses in the WB to be up to 400 bars (Coblentz, Zhou, Hillis, Richardson, & Sandiford, 1998; Gordon & Houseman, 2015). Therefore, regional stress is expected to be a dominant factor to control the fault orientation in the WB.

5 | CONCLUSIONS

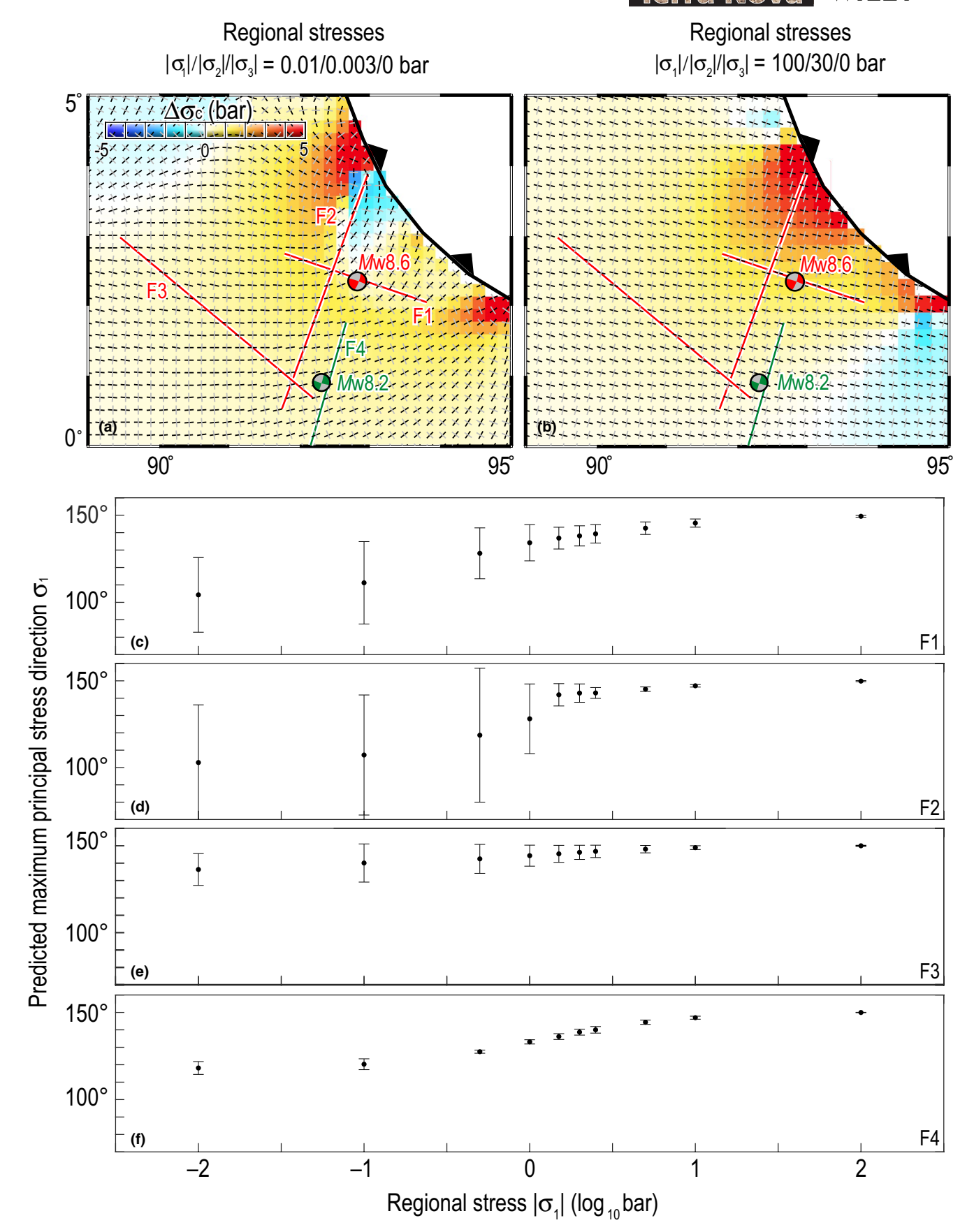
Our comprehensive stress analyses demonstrated that the 2004 earthquake has caused significant stress changes over a large region in the WB.

- The 2004 earthquake has excited widespread seismicity in the WB over hundreds of kilometres, especially within regions of calculated stress increase greater than 0.3 bar.
- 2. The 2004 earthquake caused Coulomb stress increases of 1–2.5 bars on the sub-fault F1 of the 2012 mainshock, 0.2–6.9 bars on F2, and 0–0.9 bars on F3. The 2004 earthquake also caused a stress increase of 0–0.8 bars on the rupture plane (F4) of the largest 2012 Mw8.2 aftershock. Meanwhile, the 2012 Mw8.6 imparted negative static Coulomb stress change on the Mw8.2 rupture plane. The dynamic stress triggering of the Mw8.2 aftershock by the Mw8.6 mainshock remains an alternative explanation.
- 3. For the 77 Mw ≥ 4 regional events since 2012, there was at least one nodal plane for 95% of the events, and both nodal planes of 72% of the events as promoted by the 2004 earthquake. It is interpreted that the 2004 megathrust earthquake may have promoted regional events over a large region, including these 77 events.
- 4. The regional stress directions in the WB may control the rupture orientation of the 2012 strike-slip earthquake.

ACKNOWLEDGEMENTS

The authors thank Volkan Sevilgen and Ross Stein for providing the source file of the 2004 Sumatra megathrust earthquake and the Deep Sea Geodynamics group of the SCSIO for discussion.

FIGURE 12 (a, b) Coulomb stress changes (color) on optimally oriented receiver faults in the Wharton Basin under the combination of the 2004 Sumatra coseismic stress changes and the assumed regional stress field. The magnitudes of the three components of the regional stress field are assumed for cases of $|\sigma_1|/|\sigma_2|/|\sigma_3| = 0.01/0.003/0$ bar (panel a) and $|\sigma_1|/|\sigma_2|/|\sigma_3| = 100/30/0$ bars (panel b), respectively. Black and grey short lines indicate the calculated local maximum shear stress directions for right- and left-lateral failure planes, respectively. (c-f) Calculated mean (dots) and *SD* (error bar) values of the calculated maximum principle stress directions along the 2012 sub-faults F1 (c), F2 (d), F3 (e) and F4 (f), respectively, as a function of the assumed magnitude of the regional stress $|\sigma_1|$ [Colour figure can be viewed at wileyonlinelibrary.com]



	F1		F2		F3	F3		F4	
$ \sigma_1 / \sigma_2 / \sigma_3 $ (bar)	Mean (°)	Std (°)	Mean (°)	Std (°)	Mean (°)	Std (°)	Mean (°)	Std (°)	
0.01/0.003/0	104.2	21.4	102.9	33.3	136.4	9.1	118.1	3.7	
0.1/0.03/0	111.2	22.6	107.2	33.6	140.1	10.9	120.3	3.1	
0.5/0.15/0	128.1	14.6	118.6	38.6	142.5	8.3	127.5	0.9	
1/0.3/0	134.2	10.4	128.1	20.1	144.3	6.0	133.1	1.2	
1.5/0.45/0	136.8	6.2	141.9	6.4	145.4	4.9	136.2	1.7	
2/0.6/0	138.1	5.8	142.9	5.3	146.2	4.1	138.7	1.7	
2.5/0.75/0	139.3	5.3	143.0	3.1	146.8	3.5	140.0	1.9	
5/1.5/0	142.6	3.6	145.2	1.3	148.1	2.1	144.4	1.2	
10/3/0	145.5	2.3	147.1	0.7	149.0	1.1	147.0	0.9	
100/30/0	149.4	0.5	149.8	0.3	150.0	0	150.0	0.1	

TABLE 2 Mean and *SD* values of the predicted maximum principal stress direction along sub-faults F1, F2, F3, and F4 as a function of assumed regional stresses $|\sigma_1|/|\sigma_2|/|\sigma_3|$

This research was supported by funding from the China-Pakistan Joint Research Center on Earth Sciences; Southern Marine Science and Engineering Guangdong Laboratory (Guangzhou; GML2019ZD0205); National Natural Science Foundation of China (41890813, 91628301, 41976064, and 41976066); and Chinese Academy of Sciences (Y4SL021001, QYZDY-SSW-DQC005, and 133244KYSB20180029).

CONFLICT OF INTEREST

There are no conflicts of interest to declare.

DATA AVAILABILITY STATEMENT

The data that support the findings of this study are available on request from the corresponding authors.

ORCID

Jian Lin https://orcid.org/0000-0002-6831-2014

Fan Zhang https://orcid.org/0000-0003-1608-7764

Zhiyuan Zhou https://orcid.org/0000-0002-8963-3167

REFERENCES

- Ammon, C. J., Ji, C., Thio, H.-K., Robinson, D., Ni, S., Hjorleifsdottir, V., ... Helmberger, D. (2005). Rupture process of the 2004 Sumatra-Andaman earthquake. *Science*, 308(5725), 1133–1139. https://doi. org/10.1126/science.1112260
- Anderson, G., Aagaard, B., & Hudnut, K. (2003). Fault interactions and large complex earthquakes in the Los Angeles area. *Science*, 302, 1946–1949. https://doi.org/10.1126/science.1090747
- Bird, P. (2003). An updated digital model of plate boundaries. *Geochemistry*, *Geophysics*, *Geosystems*, 4(3). https://doi.org/10.1029/2001gc000252
- Carton, H., Singh, S. C., Hananto, N. D., Martin, J., Djajadihardja, Y. S., Udrekh, ... Gaedicke, C. (2014). Deep seismic reflection images of the Wharton Basin oceanic crust and uppermost mantle offshore Northern Sumatra: Relation with active and past deformation. *Journal of Geophysical Research: Solid Earth*, 119(1), 32–51. https://doi. org/10.1002/2013jb010291
- Chlieh, M., Avouac, J.-P., Hjorleifsdottir, V., Song, T.-r A., Ji, C., Sieh, K., ... Galetzka, J. (2007). Coseismic slip and afterslip of the great Mw 9.15 Sumatra-Andaman earthquake of 2004. Bulletin of the

- Seismological Society of America, 97(1A), S152-S173. https://doi.org/10.1785/0120050631
- Coblentz, D. D., Zhou, S., Hillis, R. R., Richardson, R. M., & Sandiford, M. (1998). Topography, boundary forces, and the Indo-Australian intraplate stress field. *Journal of Geophysical Research: Solid Earth*, 103(B1), 919–931. https://doi.org/10.1029/97JB02381
- Delescluse, M., Chamot-Rooke, N., Cattin, R., Fleitout, L., Trubienko, O., & Vigny, C. (2012). April 2012 intra-oceanic seismicity off Sumatra boosted by the Banda-Aceh megathrust. *Nature*, 490(7419), 240–244. https://doi.org/10.1038/nature11520
- Deplus, C., Diament, M., Hébert, H., Bertrand, G., Dominguez, S., Dubois, J., ... Sibilla, J.-J. (1998). Direct evidence of active deformation in the eastern Indian oceanic plate. *Geology*, 26(2), 131–134. https://doi.org/10.1130/0091-7613(1998)026<0131:DEOAD I>2.3.CO:2
- Duputel, Z., Kanamori, H., Tsai, V. C., Rivera, L., Meng, L., Ampuero, J.-P., & Stock, J. M. (2012). The 2012 Sumatra great earthquake sequence. *Earth and Planetary Science Letters*, 351, 247–257. https://doi.org/10.1016/j.epsl.2012.07.017
- Dziewoński, A., Chou, T. A., & Woodhouse, J. (1981). Determination of earthquake source parameters from waveform data for studies of global and regional seismicity. *Journal of Geophysical Research: Solid Earth*, 86(B4), 2825–2852. https://doi.org/10.1029/JB086iB04p02825
- Ekström, G., Nettles, M., & Dziewoński, A. (2012). The global CMT project 2004–2010: Centroid-moment tensors for 13,017 earthquakes. *Physics of the Earth and Planetary Interiors*, 200, 1–9. https://doi.org/10.1016/j.pepi.2012.04.002
- Fan, W., & Shearer, P. M. (2016). Fault interactions and triggering during the 10 January 2012 Mw7.2 Sumatra earthquake. *Geophysical Research Letters*, 43(5), 1934–1942. https://doi.org/10.1002/2016gl067785
- Freed, A. M. (2005). Earthquake triggering by static, dynamic, and postseismic stress transfer. *Annual Review of Earth and Planetary Sciences*, 33, 335–367. https://doi.org/10.1146/annurev.earth.33.092203.122505
- Gomberg, J., Bodin, P., & Reasenberg, P. (2003). Observing earthquakes triggered in the near field by dynamic deformations. Bulletin of Seismological Society of America, 93, 118–138. https://doi. org/10.1785/0120020075
- Gordon, R. G., & Houseman, G. A. (2015). Deformation of Indian Ocean lithosphere: Evidence for a highly nonlinear rheological law. *Journal of Geophysical Research*: *Solid Earth*, 120(6), 4434–4449. https://doi.org/10.1002/2015jb011993
- Heidbach, O., Rajabi, M., Cui, X., Fuchs, K., Müller, B., Reinecker, J., ... Zoback, M. (2018). The world stress map database release 2016:

- Crustal stress pattern across scales. *Tectonophysics*, 744, 484–498. https://doi.org/10.1016/j.tecto.2018.07.007
- Hill, D. P., Reasenberg, P. A., Michael, A., Arabaz, W. J., Beroza, G., Brumbaugh, D., ... Zollweg, J. (1993). Seismicity remotely triggered by the magnitude 7.3 Landers, California, Earthquake. Science, 260, 1617–1623. https://doi.org/10.1126/science.260.5114.1617
- Hill, E. M., Yue, H., Barbot, S., Lay, T., Tapponnier, P., Hermawan, I., ... Sieh, K. (2015). The 2012 Mw8.6 Wharton Basin sequence: A cascade of great earthquakes generated by near-orthogonal, young, oceanic mantle faults. *Journal of Geophysical Research: Solid Earth*, 120(5), 3723–3747. https://doi.org/10.1002/2014jb011703
- Ishii, M., Kiser, E., & Geist, E. L. (2013). Mw 8.6 Sumatran earthquake of 11 April 2012: Rare seaward expression of oblique subduction. *Geology*, 41(3), 319–322. https://doi.org/10.1130/g33783.1
- Jacob, J., Dyment, J., & Yatheesh, V. (2014). Revisiting the structure, age, and evolution of the Wharton Basin to better understand subduction under Indonesia. *Journal of Geophysical Research*: *Solid Earth*, 119(1), 169–190. https://doi.org/10.1002/2013jb010285
- King, G. C., & Cocco, M. (2001). Fault interaction by elastic stress changes: New clues from earthquake sequences. Advances in Geophysics, 44, 1–38. https://doi.org/10.1016/S0065 -2687(00)80006-0
- King, G. C., Stein, R. S., & Lin, J. (1994). Static stress changes and the triggering of earthquakes. Bulletin of Seismological Society of America, 84(3), 935–953. https://doi.org/10.1016/0148-9062(95)94484-2
- Lay, T. (2019). Reactivation of oceanic fracture zones in large intraplate earthquakes? Transform Plate Boundaries and Fracture Zones, 89–104. https://doi.org/10.1016/b978-0-12-812064-4.00004-9
- Lay, T., Kanamori, H., Ammon, C. J., Nettles, M., Ward, S. N., Aster, R. C., ... Butler, R. (2005). The great Sumatra-Andaman earthquake of 26 December 2004. Science, 308(5725), 1127–1133. https://doi.org/10.1126/science.1112250
- Lin, J., & Stein, R. S. (2004). Stress triggering in thrust and subduction earthquakes and stress interaction between the southern San Andreas and nearby thrust and strike-slip faults. *Journal of Geophysical Research*: *Solid Earth*, 109(B2). https://doi.org/10.1029/2003JB002607
- Lin, J., Stein, R. S., Meghraoui, M., Toda, S., Ayadi, A., Dorbath, C., & Belabbes, S. (2011). Stress transfer among en echelon and opposing thrusts and tear faults: Triggering caused by the 2003 Mw=6.9 Zemmouri, Algeria, earthquake. *Journal of Geophysical Research: Solid Earth*, 116(B3). https://doi.org/10.1029/2010jb007654
- Liu, C.-S., Curray, J. R., & McDonald, J. (1983). New constraints on the tectonic evolution of the eastern Indian Ocean. Earth and Planetary Science Letters, 65(2), 331–342. https://doi.org/10.1016/0012-821X(83)90171-1
- Meng, L., Ampuero, J.-P., Stock, J., Duputel, Z., Luo, Y., & Tsai, V. (2012). Earthquake in a maze: Compressional rupture branching during the 2012 Mw 8.6 Sumatra earthquake. *Science*, 337(6095), 724–726. https://doi.org/10.1126/science.1224030
- Qiu, Q., & Chan, C.-H. (2019). Coulomb stress perturbation after great earthquakes in the Sumatran subduction zone: Potential impacts in the surrounding region. *Journal of Asian Earth Sciences*, 180. https://doi.org/10.1016/j.jseaes.2019.103869
- Robinson, D., Henry, C., Das, S., & Woodhouse, J. (2001). Simultaneous rupture along two conjugate planes of the Wharton Basin earthquake. *Science*, 292(5519), 1145–1148. https://doi.org/10.1126/science.1059395

- Sevilgen, V., Stein, R. S., & Pollitz, F. F. (2012). Stress imparted by the great 2004 Sumatra earthquake shut down transforms and activated rifts up to 400 km away in the Andaman Sea. Proceedings of the National Academy of Sciences of the United States of America, 109(38), 15152–15156. https://doi.org/10.1073/pnas.1208799109
- Singh, S. C., Hananto, N., Qin, Y., Leclerc, F., Avianto, P., Tapponnier, P. E., ... Barbot, S. (2017). The discovery of a conjugate system of faults in the Wharton Basin intraplate deformation zone. *Science Advances*, 3(1), e1601689. https://doi.org/10.1126/sciadv.1601689
- Toda, S., Stein, R. S., & Lin, J. (2011). Widespread seismicity excitation throughout central Japan following the 2011 M=9.0 Tohoku earthquake and its interpretation by Coulomb stress transfer. *Geophysical Research Letters*, 38(7). https://doi.org/10.1029/2011gl047834
- Toda, S., Stein, R. S., Sevilgen, V., & Lin, J. (2011). Coulomb 3.3 graphic-rich deformation and stress-change software for earthquake, tectonic, and volcano research and teaching-user guide. U. S. Geological Survey, Open-File Report 2011–1060. https://doi.org/10.3133/ofr20111060
- Wang, D., Mori, J., & Uchide, T. (2012). Supershear rupture on multiple faults for the Mw8.6 off Northern Sumatra, Indonesia earthquake of April 11, 2012. *Geophysical Research Letters*, 39(21). https://doi.org/10.1029/2012gl053622
- Wei, S., Helmberger, D., & Avouac, J.-P. (2013). Modeling the 2012 Wharton basin earthquakes off-Sumatra: Complete lithospheric failure. *Journal of Geophysical Research: Solid Earth*, 118(7), 3592–3609. https://doi.org/10.1002/jgrb.50267
- Wu, J., Lei, D., Cai, Y., & Li, H. (2015). Stress triggering of the 2012 Sumatra Mw 8.2 earthquake by the 2012 Sumatra Mw 8.6 earthquake. The Electronic Journal of Geotechnical Engineering, 20(1), 213–219.
- Yue, H., Lay, T., & Koper, K. D. (2012). En échelon and orthogonal fault ruptures of the 11 April 2012 great intraplate earthquakes. *Nature*, 490(7419), 245–249. https://doi.org/10.1038/nature11492
- Zhang, H., Chen, J., & Ge, Z. (2012). Multi-fault rupture and successive triggering during the 2012 Mw 8.6 Sumatra offshore earthquake. Geophysical Research Letters, 39(22). https://doi.org/10.1029/2012g 1053805

SUPPORTING INFORMATION

Additional supporting information may be found online in the Supporting Information section.

Fig S1. Maximum Coulomb stress changes on optimally-oriented strike-slip receiver faults caused by the 2004 Mw9.2 earthquake, assuming $\mu'=0$ (a), $\mu'=0.2$ (b), $\mu'=0.6$ (c), and $\mu'=0.8$ (d). The contour of 0.1 bar is in red and the contour of 0.3 bar is in black. Small circles show the events during 12/26/2004-04/10/2012.

How to cite this article: Guo L, Lin J, Zhang F, Zhou Z. Transfer of stress from the 2004 Mw9.2 Sumatra subduction earthquake promoted widespread seismicity and large strike-slip events in the Wharton Basin. *Terra Nova*. 2021;33:74–85. https://doi.org/10.1111/ter.12492